Molecular Cell, Volume *82*

Supplemental information

Receptor tyrosine kinases regulate signal transduction through a liquid-liquid phase separated state

Chi-Chuan Lin, Kin Man Suen, Polly-Anne Jeffrey, Lukasz Wieteska, Jessica A. Lidster, Peng Bao, Alistair P. Curd, Amy Stainthorp, Caroline Seiler, Hans Koss, Eric Miska, Zamal Ahmed, Stephen D. Evans, Carmen Molina-París, and John E. Ladbury

SUPPLEMENTAL INFORMATION

Receptor tyrosine kinases regulate signal transduction through a liquid–liquid phase separated state

Chi-Chuan Lin, Kin Man Suen, Polly-Anne Jeffrey, Lukasz Wieteska, Jessica A. Lidster, Peng Bao, Alistair P. Curd, Amy Stainthorp, Caroline Seiler, Hans Koss, Eric Miska, Zamal Ahmed, Stephen D. Evans, Carmen Molina-París, and John E. Ladbury

Supplementary Figure 1

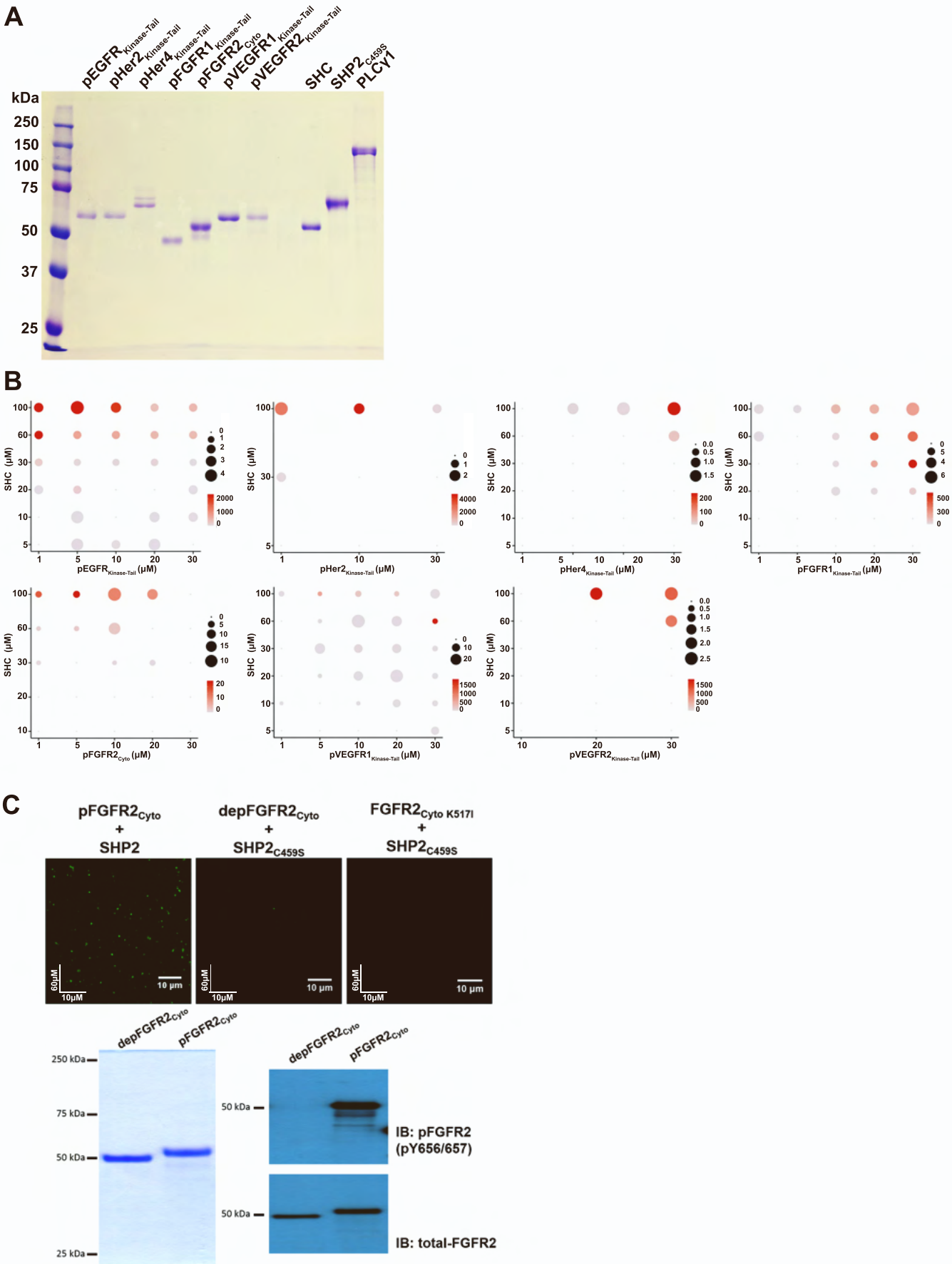

Figure S1. Preparation of recombinant proteins and phosphorylation-dependent FGFR2-SHP2 droplet formation, Related to Figure 1.

(A) Coomassie blue staining of purified recombinant proteins used in this study. Proteins were expressed and purified from *E.coli* (see Material and Methods) and the purity was greater than 95% examined by SDS-PAGE electrophoresis.

(B) Phase diagrams of phosphorylated EGFR, FGFR, and VEGFR family proteins (Atto-488 labelled) with concentrations shown in X-axis and SHC (Y-axis) in 20 mM HEPES (pH 7.5), 150 mM NaCl, and 1 mM TCEP. The sizes of the circles represent the average sizes of droplets (μm^2) and the colour scale bars represent the numbers of droplets in a 0.0256 mm^2 area.

(C) (Top panel) Replacement of $SHP2_{C459S}$ with wild type SHP2 under identical conditions results in the reduction of droplet size. Unphosphorylated $FGFR2_{Cyto}$ (dep$FGFR2_{Cyto}$ or $FGFR2_{Cyto\ K517I}$ (the kinase-dead mutant)) cannot form droplets with $SHP2_{C459S}$. These images highlight the requirement for prolonged phosphorylation on $FGFR2_{Cyto}$ for droplet formation. (Below) The phosphorylation state of $FGFR2_{Cyto}$ was examined by a gel shift assay (left, coomassie blue staining) and an immunoblotting (right) using a specific phospho-antibody (pY656/657) against the activation loop of FGFR2.

Supplementary Figure 2

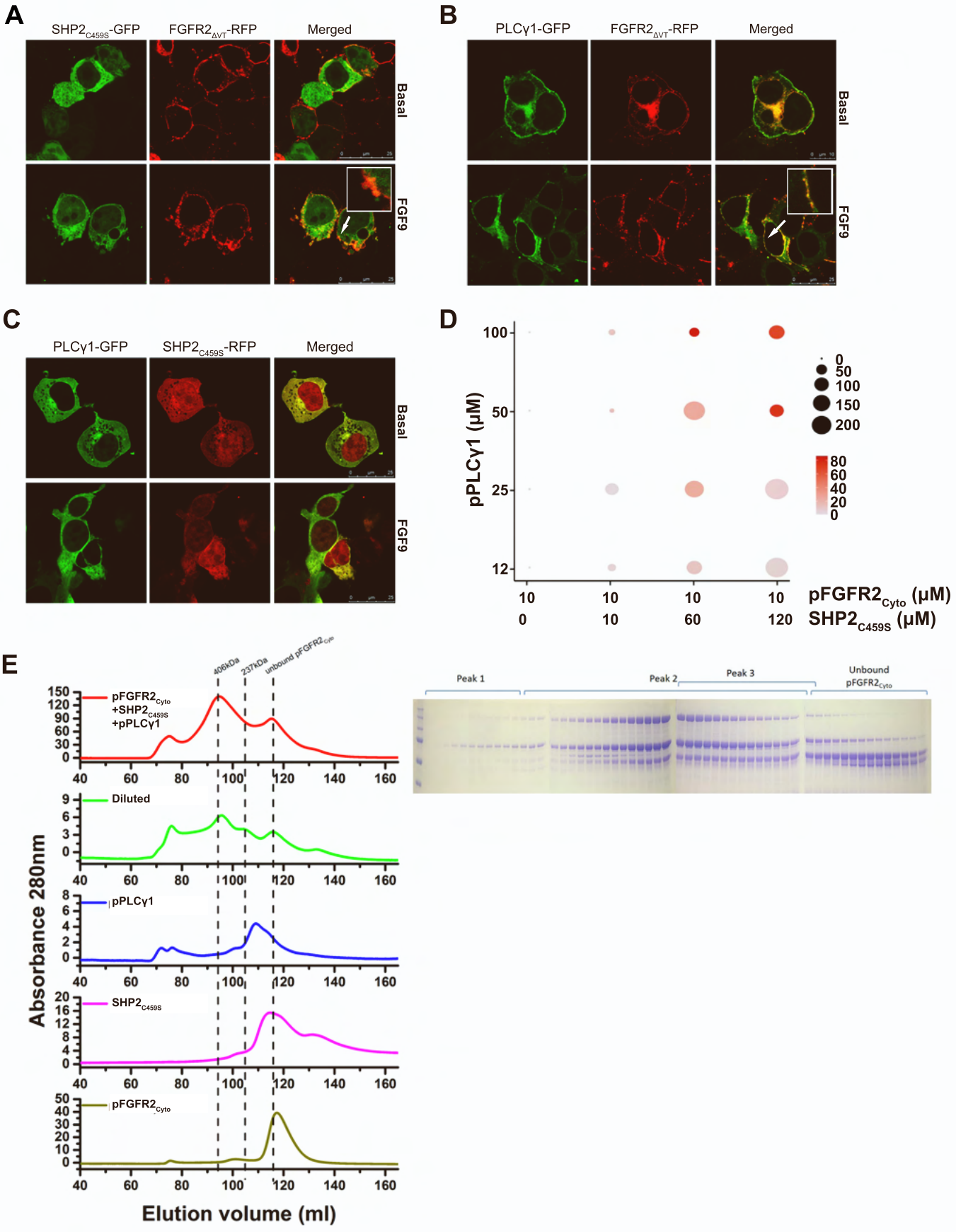

Figure S2. FGFR2-SHP2-PLCγ1 complex formation in cells and *in vitro*, Related to Figure 2.

(A) Cell images showing $FGFR2_{\Delta VT}$-RFP and $SHP2_{C459S}$-GFP cluster formation upon FGFR2 expression and activation (stimulated by FGF9) in HEK293T cells. Insets: magnification of regions shown by arrow to exemplify $FGFR2_{\Delta VT}$-RFP and $SHP2_{C459S}$-GFP clusters.

(B) Cell images showing $FGFR2_{\Delta VT}$-RFP and PLCγ1-GFP cluster formation upon FGFR2 expression and activation (stimulated by FGF9) in HEK293T cells. Insets: magnification of regions shown by arrow to exemplify $FGFR2_{\Delta VT}$-RFP and PLCγ1-GFP clusters.

(C) No evidence of SHP2 or PLCγ1 cluster formation in the absence of $FGFR2_{\Delta VT}$; both SHP2 and PLCγ1 appear to randomly diffuse in cytosol.

(D) Phase diagrams of phosphorylated $pFGFR2_{Cyto}$-$SHP2_{C459S}$-pPLCγ1 in 20 mM HEPES (pH7.5), 150 mM NaCl, and 1 mM TCEP. $pFGFR2_{Cyto}$ was labelled with Atto 488, $SHP2_{C459S}$ was labelled with Atto 550 and pPLCγ1 was labelled with Atto 647. 10 μM of $pFGFR2_{Cyto}$ was mixed with various concentrations of $SHP2_{C459S}$ (0, 10, 60, and 120 μM) first before the addition of pPLCγ1 (from 100 – 12 μM). The sizes of the circles represent the average sizes of droplets (μm^2) and the colour scale bars represent the numbers of droplets in a 0.0256 mm^2 area. In the absence of $SHP2_{C459S}$, $pFGFR2_{Cyto}$ does not form droplets with pPLCγ1.

(E) Size exclusion chromatography was used to isolate the $pFGFR2_{Cyto}$-$SHP2_{C459S}$-pPLCγ1 complex. The components of each elution fraction were examined by coomassie gel staining. A complex of greater than 1:1:1 of $pFGFR2_{Cyto}$-$SHP2_{C459S}$-pPLCγ1 ternary complex was observed with a calculated molecular weight of 406 kDa (peak 2). The binary $pFGFR2_{Cyto}$-$SHP2_{C459S}$ complex was identified as peak 3 (237kDa).

Supplementary Figure 3

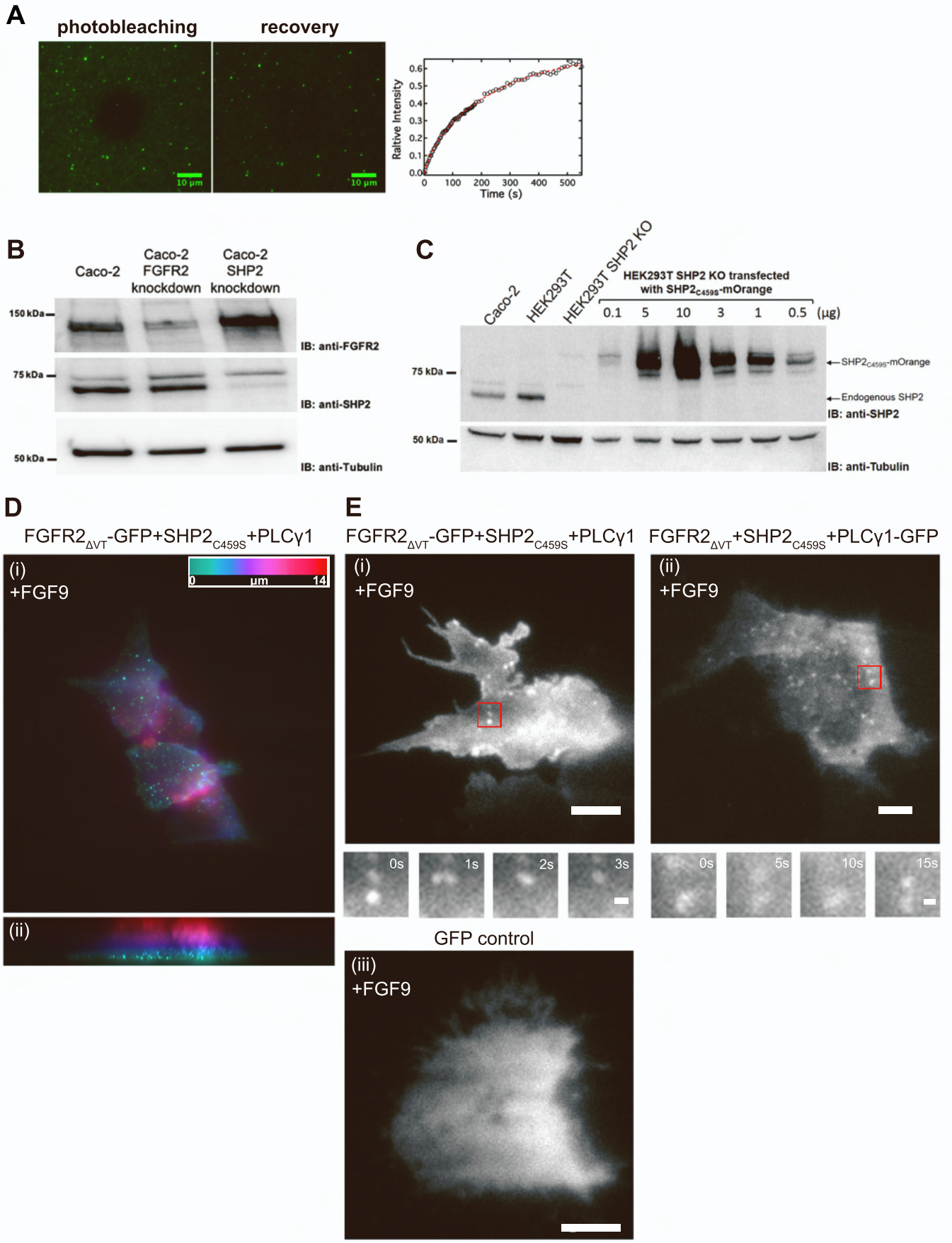

Figure S3. The formation of FGFR2-SHP2-PLCγ1 complex on membranes, Related to Figure 3.

(A) FRAP of pFGFR2$_{Cyto}$ (labelled with Atto 488) on supported lipid bilayers to demonstrate the liquid-like property. Left panel: photobleaching, middle panel: fluorescent recovery after bleaching, and right panel: real time quantification of FRAP data for pFGFR2$_{Cyto}$.

(B) The knockdown levels of endogenous FGFR2 and SHP2 was examined by immunoblotting.

(C) The average exogenous expression level of SHP2$_{C459S}$ in HEK293T SHP2 KO cells was adjusted in order to mimic the endogenous SHP2 expression.

(D) HILO image showing that the FGFR2$_{\Delta VT}$-EGFP droplets (coexpressed with untagged SHP2$_{C459S}$ and PLCγ1; stimulated with 10ng/ml FGF9) are localised close to the coverslip (improved contrast in HILO microscopy. Data were presented as depth-coded images ((i): XY view and (ii): XZ view), colour bar: 0-14μm. In the XZ view (ii), it is clear that many of the droplets, at different brightnesses, are visible along the flat line of the coverslip, and hence localised on the plasma membrane.

(E) HILO image showing that: (i) fusion event of FGFR2$_{\Delta VT}$-EGFP droplets (coexpressed with untagged SHP2$_{C459S}$ and PLCγ1; stimulated with 10 ng/ml FGF9) on the membrane. The four time lapse images were monitored from the red box shown in the whole cell image. Scale bar for the whole cell image: 5 μm; scale bar for the time lapse image: 500 nm. (ii) fusion/fission event of PLCγ1-EGFP droplets (coexpressed with untagged FGFR2$_{\Delta VT}$ and SHP2$_{C459S}$; stimulated with 10 ng/ml FGF9) on the membrane. The four time lapse images were monitored from the red box shown in the whole cell image. Scale bar for the whole cell image: 5 μm; scale bar for the time lapse image: 500 nm. (iii) EGFP alone control. No droplet formation. Scale bar: 5 μm

Supplementary Figure 4

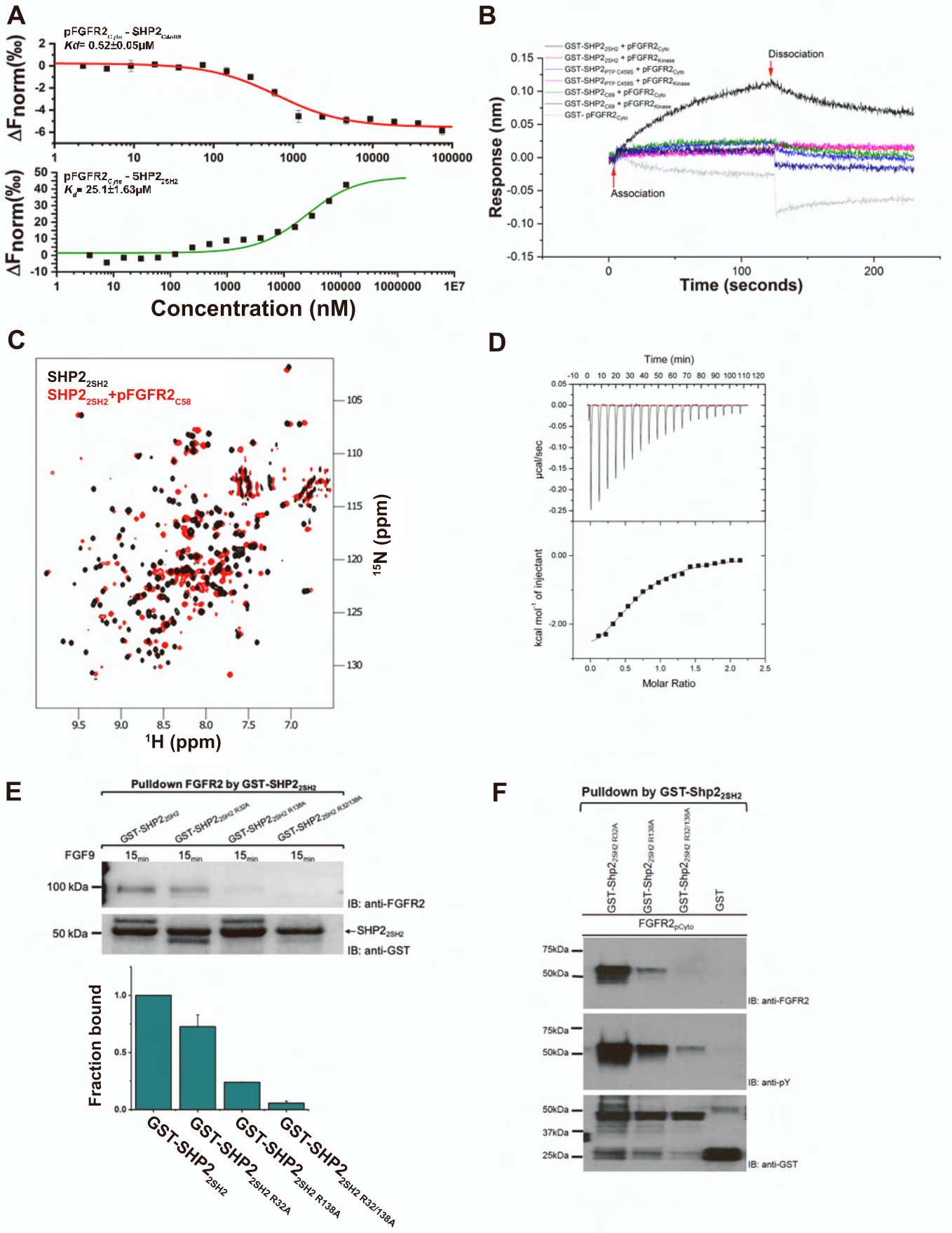

Figure S4. The molecular interaction of FGFR2 with SHP2, Related to Figure 4.

(A) MST isotherm for the binding of $pFGFR2_{Cyto}$ to full length $SHP2_{C459S}$ (K_d = 0.52±0.0 μM; red curve) or the truncated tandem SH2 domain $SHP2_{2SH2}$ (K_d = 25.1±1.63 μM; green curve).

(B) BLI experiments were used to confirm the phosphorylation-dependent interaction and the specific domains required for binding. GST-$SHP2_{2SH2}$, GST-$SHP2_{PTP\ C459S}$ and GST-$SHP2_{C69}$ were immobilized on GST sensors and $pFGFR2_{Cyto}$ (5 μM) and $pFGFR2_{Kinase}$ (5 μM) were used to test the binding. $pFGFR2_{Cyto}$ clearly interacts with GST-$SHP2_{2SH2}$. The expected weak binding to $pFGFR2_{Kinase}$ is not visible due to the concentration of this reagent being below the K_d for the interaction. Black - immobilized GST-$SHP2_{2SH2}$ with $pFGFR2_{Cyto}$; red - immobilized GST-$SHP2_{2SH2}$ with $pFGFR2_{Kinase}$; blue - immobilized GST-$SHP2_{PTP\ C459S}$ with $pFGFR2_{Cyto}$; pink - immobilized GST-$SHP2_{PTP\ C459S}$ with $pFGFR2_{Kinase}$; green - immobilized GST-$SHP2_{C69}$ with $pFGFR2_{Cyto}$; dark blue - immobilized GST-$SHP2_{C69}$ with $pFGFR2_{Kinase}$; grey - immobilized GST with $pFGFR2_{Cyto}$. Ligand-analyte association (0 sec) and dissociation (buffer washing, 120 sec) are indicated by red arrows.

(C) NMR spectra of 1^H, 15^N-labelled isolated $SHP2_{2SH2}$ (100 μM, black) and with added $pFGFR2_{C58}$ (300 μM, red). The chemical shifts for individual residues (i.e. movement of peaks from black to red positions) confirm direct interaction across a broad interface.

(D) Binding of $SHP2_{2SH2}$ (10 μM) with the $pFGFR2_{C58}$ (100 μM) shown by ITC. The top panel shows raw data for the titration; the bottom panel shows integrated peaks plotted on axes with molar heat of binding versus the molar ratio of titrated protein fitted to a single-site binding model. Heats of dilution were measured in a separate control experiment and subtracted from binding data prior to fitting. Importantly the stoichiometry of the interaction 1:1 confirms that only CSH2 from the tandem SH2 domains recognizes pY769 on the receptor.

(E) (Top) GST-$SHP2_{2SH2}$, GST-$SHP2_{2SH2\ R32A}$, GST-$SHP2_{2SH2\ R138A}$ and GST-$SHP2_{2SH2\ R32/138A}$ were used to pull down $FGFR2_{\Delta VT}$ from HEK293T cells stimulated with FGF9 (10 ng/ml). Mutation of R138 abrogates binding of FGFR2 confirming the requirement of the wild type

CSH2 domain for binding to receptor. (Bottom) Densitometry analysis of GST pull down. n=2. Data were presented as mean ± SD. Replicate data shown in Data S1E.

(F) GST-SHP2$_{2SH2}$ R32A, GST-SHP2$_{2SH2}$ R138A and GST-SHP2$_{2SH2\ R32/138A}$ were used to pull down recombinant pFGFR2$_{Cyto}$. Mutation of R138 abrogates binding of FGFR2 confirming the requirement of a wild type CSH2 domain for binding to receptor.

Supplementary Figure 5

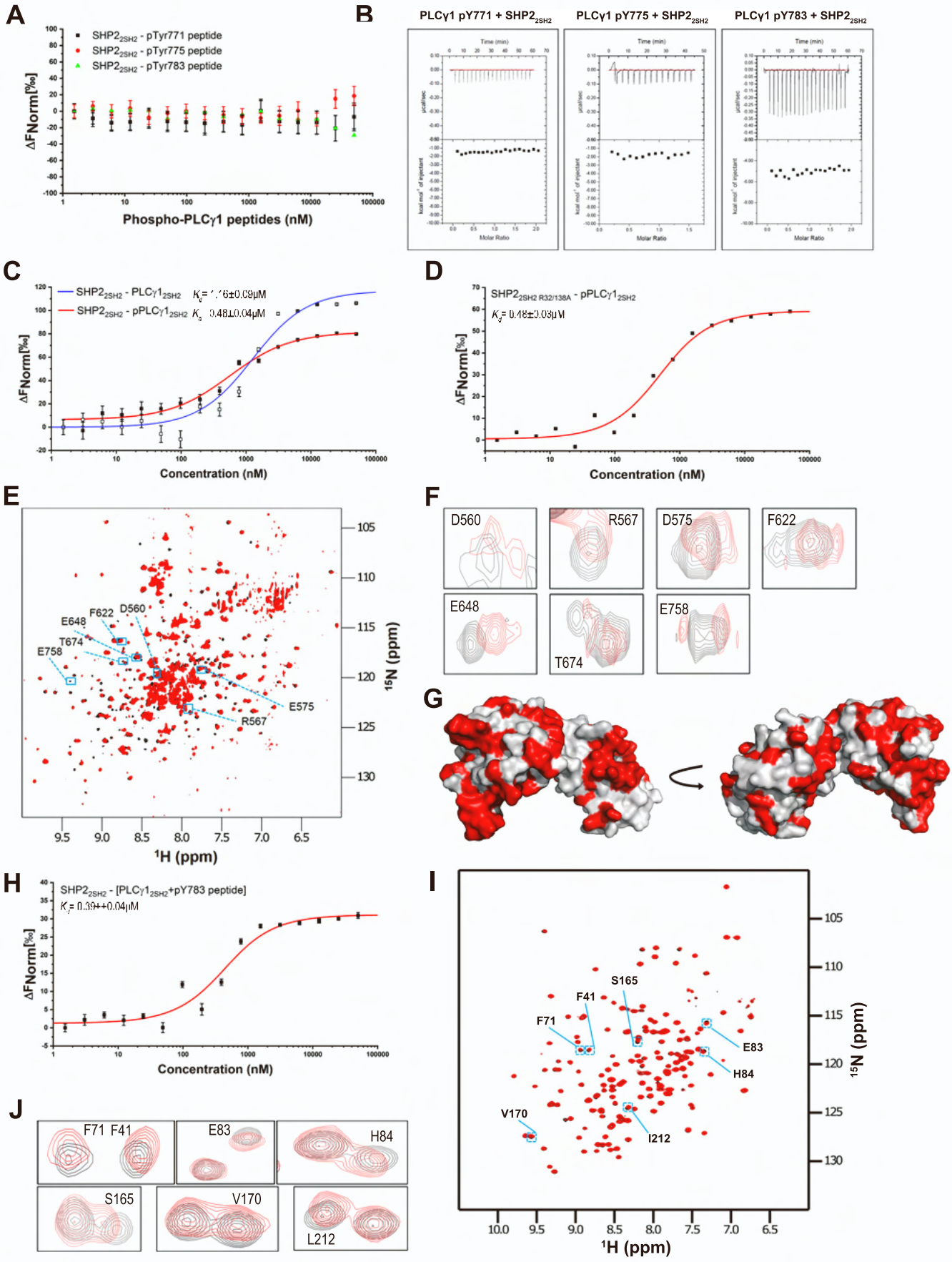

Figure S5. The molecular interaction of SHP2 with PLCγ1, Related to Figure 5.

(A) MST isotherm for the binding of synthesized PLCγ1-derived tyrosyl phosphopeptides containing pY771, pY775 or pY783 to labelled $SHP2_{2SH2}$. No significant interaction was found with any of the phosphopeptides.

(B) ITC isotherms of $SHP2_{2SH2}$ binding to PLCγ1 pY771, pY775, and pY783 tyrosyl phosphopeptides. Twenty 3 µl injections of each phosphopeptide (100 µM) were titrated into $SHP2_{2SH2}$ (10 µM) at 25°C. Top, baseline-corrected power-versus-time plot for the titration. Bottom, integrated heats and curve fitting using Origin™ software.

(C) MST measurement of $SHP2_{2SH2}$ binding to labelled $PLCγ1_{2SH2}$, blue curve; or labelled $pPLCγ1_{2SH2}$, red curve. No significant difference was observed in their binding affinities to $SHP2_{2SH2}$.

(D) MST isotherm for the interaction of labelled $SHP2_{2SH2\ R32/138A}$ mutant and $pPLCγ1_{2SH2}$, showing that the interaction is not based on the canonical binding of pY to an SH2 domain.

(E) NMR ^{1H} and ^{15N} chemical shift changes on addition of $SHP2_{2SH2}$ (600 µM) to ^{15N}-labelled $PLCγ1_{2SH2}$ (200 µM). Blue squares highlight some of the residues on the spectrum showing shift changes; which are magnified in (F).

(G) ^{1H}, ^{15N} peak assignments mapped onto the space-filling model crystal structure of $PLCγ1_{2SH2}$ (PDB code: 4FBN). The orientations of the structure are as shown in Fig. 5B. The coverage of assigned residues of $PLCγ1_{2SH2}$ is 46.5% (red, assigned residues).

(H) MST isotherm for the interaction of labelled $SHP2_{2SH2}$ and a preformed complex between $PLCγ1_{2SH2}$ and a tyrosyl phosphopeptide containing pY783 showing that the binding of pY783 does not hinder the tandem SH2 domain interface.

(I) NMR ^{1H} and ^{15N} chemical shift changes on addition of $PLCγ1_{2SH2}$ (600 µM) to ^{15N}-labelled $SHP2_{2SH2}$ (100 µM). Blue squares highlight some of the residues on the spectrum showing shift changes; which are expanded in (J).

Supplementary Figure 6

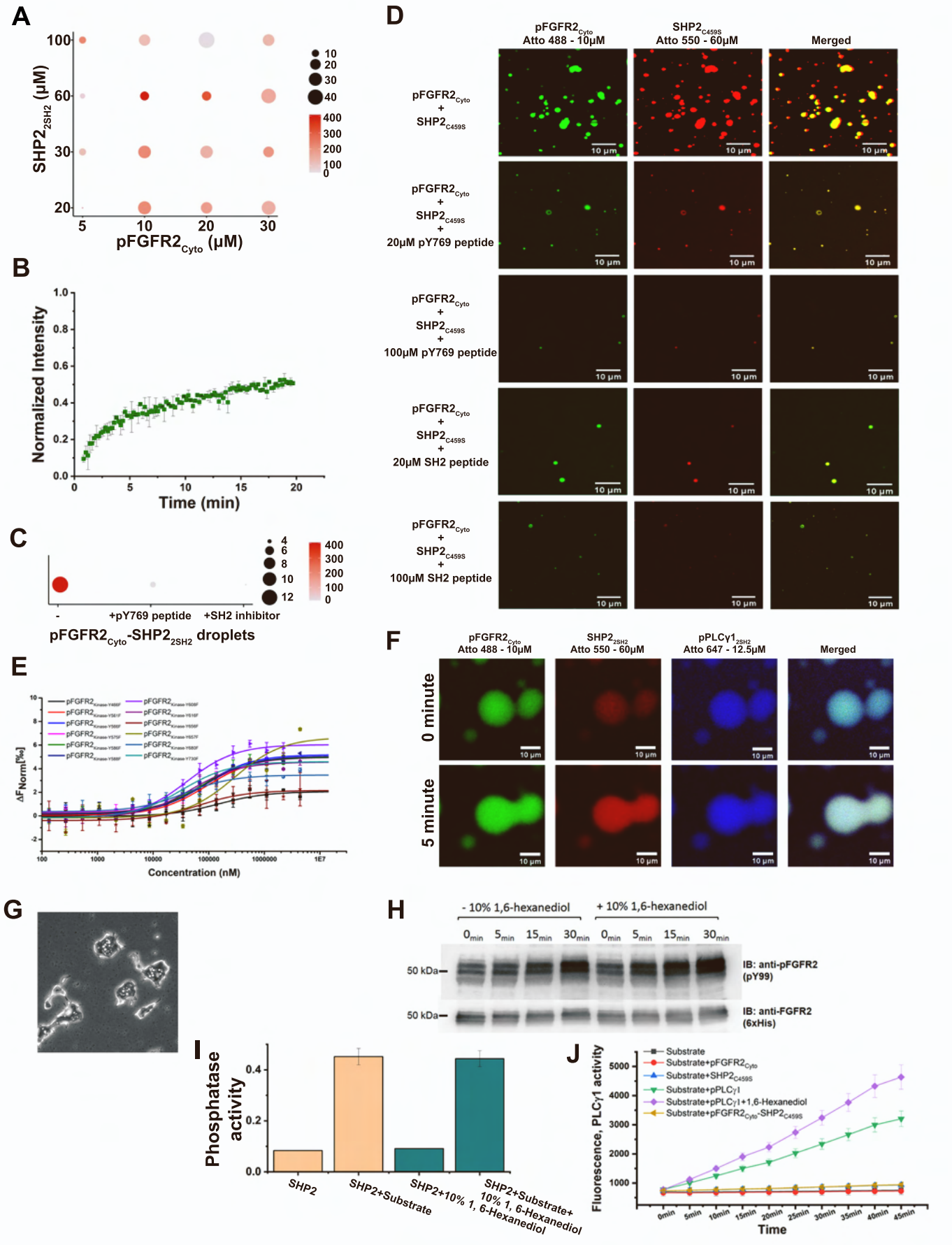

Figure S6. Characterization of FGFR2-SHP2-PLCγ1 droplets properties, Related to Figure 6.

(A) Phase diagram of $pFGFR2_{Cyto}$-Atto 488 and $SHP2_{2SH2}$-Atto 550 droplet formation in a buffer containing 20 mM HEPES (pH7.5), 150 mM NaCl, and 1 mM TCEP. The sizes of the circles represent the average sizes of droplets (μm^2) and the colour scale bars represent the numbers of droplets in a 0.0256 mm^2 area.

(B) FRAP recovery curve for $pFGFR2_{Cyto}$-Atto 488 and $SHP2_{2SH2}$ (means ± SD, n = 2 experiments).

(C) Phase diagram of $pFGFR2_{Cyto}$-Atto 488 and $SHP2_{2SH2}$-Atto 550 droplet formation with 20 μM of pY769 peptide and SH2 inhibitor peptide in a buffer containing 20 mM HEPES (pH7.5), 150 mM NaCl, and 1 mM TCEP. The addition of both inhibitor abolishes the formation of droplets. The sizes of the circles represent the average sizes of droplets (μm^2) and the colour scale bars represent the numbers of droplets in a 0.0256 mm^2 area.

(D) Inhibition of $pFGFR2_{Cyto}$-Atto 488 (10 μM) and $SHP2_{C459S}$-Atto 550 (30 μM) droplet formation by 20 μM or 100 μM of pY769 peptide or SH2 inhibitor peptide. Scale bar = 10 μm.

(E) MST measurements of $SHP2_{2SH2\ R138A}$ binding to $pFGFR2_{Kinase}$ with single Y to F mutants of all of the individual tyrosines on the kinase domain. This result shows multivalent, weak binding between SHP2 NSH2 domain and any of the available pY residues.

(F) The dynamic LLPS property of $pFGFR2_{Cyto}$ (10 μM)-$SHP2_{2SH2}$ (30 μM)-$PLCγ1_{2SH2}$ (12 μM) droplets was monitored by the fusion experiment. This experiment demonstrated the tandem SH2 domains of SHP2 and PLCγ1 are the minimum requirement to form LLPS droplets with $pFGFR2_{Cyto}$. Scale bar = 10 μm.

(G) The white light image of $pFGFR2_{Cyto}$-SHP2-PLCγ1 droplets used for enzymatic assay.

(H) Purified $pFGFR2_{Cyto}$ (10 μM) was incubated with ATP/$MgCl_2$ (5 mM) in the presence or absence of 10% 1,6-hexanediol in a buffer containing 20 mM HEPES (pH7.5), 150 mM NaCl,

and 1 mM TCEP. The effect of 1,6-hexanediol on $pFGFR2_{Cyto}$ activity was monitored by pFGFR2 immunoblotting at different time points as indicated. This result demonstrated that 10% 1,6-hexanediol does not affect kinase activity in the LLPS condition.

(I) Purified SHP2 (60 μM) was incubated with a phospho-substrate (Methods: *In vitro* phosphatase assay) in the presence or absence of 10% 1,6-hexanediol in a buffer containing 20 mM HEPES (pH7.5), 150 mM NaCl, and 1 mM TCEP. The effect of 1,6-hexanediol on SHP2 activity was monitored by the turnover rate of the substrate. This result demonstrated that 10% 1,6-hexanediol does not affect phosphatase activity in the LLPS condition. n=2. Data were presented as mean ± SD.

(J) Purified $pFGFR2_{Cyto}$ (10 μM), $SHP2_{C459S}$ (60 μM), and pPLCγ1 (50 μM) were incubated with artificial pPLCγ1 substrate 4-methylumbelliferyl myo-inositol-1-phosphate, N-methyl-morpholine salt in a buffer containing 20mM HEPES (pH7.5), 150mM NaCl, and 1mM TCEP to test the specificity of $pFGFR2_{Cyto}$, $SHP2_{C459S}$, and pPLCγ1 with the substrate. $SHP2_{C459S}$ shows a low level of nonspecific reaction (blue and brown curves). The addition of 10% 1,6-hexanediol upregulates pPLCγ1 activity (purple curve) comparing with pPLCγ1 alone (green curve). Sample sizes = 8, Data were presented as mean ± SD.

Supplementary Figure 7

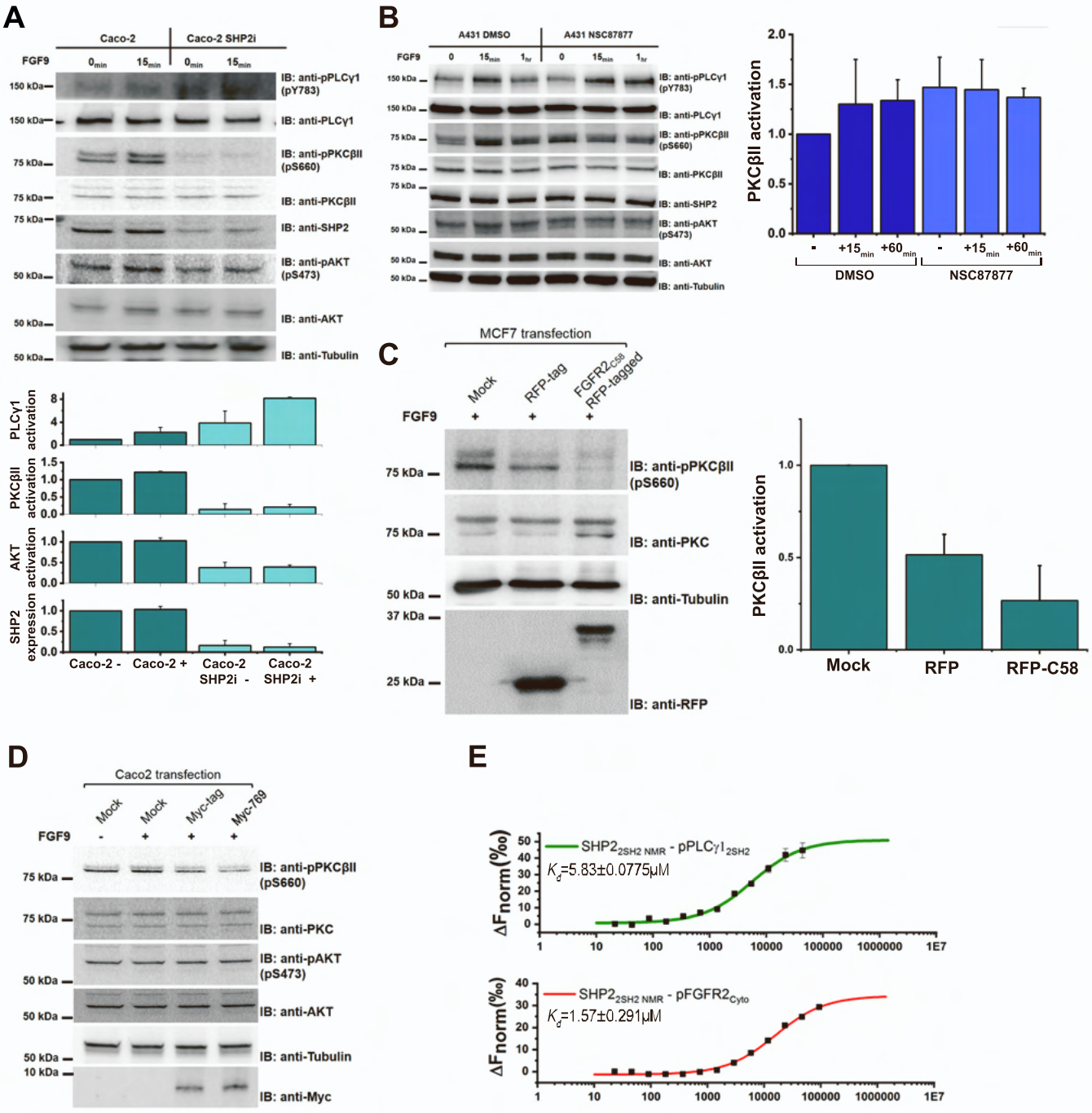

Figure S7. FGFR2-SHP2-PLCγ1 signalling regulated by phase separation, Related to Figure 7.

(A) (Top) Western blot showing Caco-2 cells with knock down of SHP2 (Caco-2 SHP2i). As seen in MCF7 SHP2 KO and A431 SHP2i cells the phosphorylation of PLCγ1 Y783 is increased on FGF9 stimulation (10 ng/ml) of FGFR2. Phosphorylation of S660 on PKCβII and S473 on AKT act as markers for up-regulation of PLCγ1 signalling. This is suppressed in the absence of SHP2 in the Caco-2 SHP2i cells. (Bottom) Densitometry analysis of SHP2 expression and the activation levels of various signalling proteins (dark cyan: parental cells; light cyan: SHP2 depletion cells). n=2. Data were presented as mean ± SD. Replicate data shown in Data S3D.

(B) (Left) Western blot showing the presence of phosphorylated downstream effector proteins in A431 cells without (using only DMSO vehicle) or with 50 μM of NSC87877 SHP2 inhibitor. The negligible change of phosphorylation of PKCβII and AKT upon FGF9 stimulation (10 ng/ml) shows that SHP2 phosphatase activity does not affect PLCγ1 activity. (Right) Densitometry analysis of the activation levels of various signalling proteins (dark blue: DMSO treatment; light blue: NSC87877 SHP2 inhibitor treatment). n=3. Data were presented as mean ± SD. Replicate data shown in Data S3E.

(C) (Left) Transfection of RFP-tagged $FGFR2_{C58}$ to FGF9-stimulated (10 ng/ml) MCF7 cells results in the down regulation of PKCβII activity. (Right) Densitometry analysis of PKCβII activity. n=3. Data were presented as mean ± SD. Replicate data shown in Data S3F.

(D) Transfection of Myc-tagged FGFR2 pY769 peptide to Caco-2 cells followed by stimulation of FGF9 (10 ng/ml) results in the down regulation of PKCβII activity, but has no effect on AKT activity.

(E) MST isotherm for the binding of $SHP2_{2SH2\ NMR.}$ The mutations on the interface decrease the interaction with $pPLC\gamma1_{2SH2}$ with an affinity of 5.83±0.077 μM (green curve) compared with wild

type $SHP2_{2SH2}$ (K_d = 0.48±0.0 4μM; Fig. S5C), but it does not affect the interaction with $pFGFR2_{Cyto}$ (K_d = 15.7±0.291 μM; red curve).

Data S1. Replicated western blots, Related to Figure 4 and Figure S4.

A

Figure 4A replicate 2

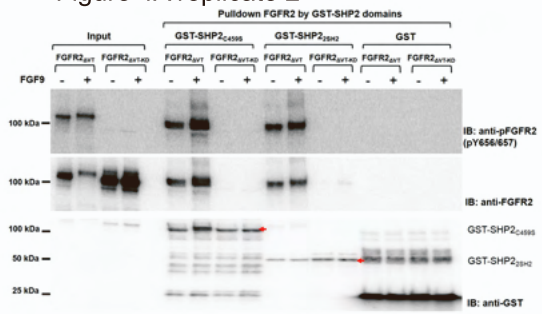

Figure 4A replicate 3

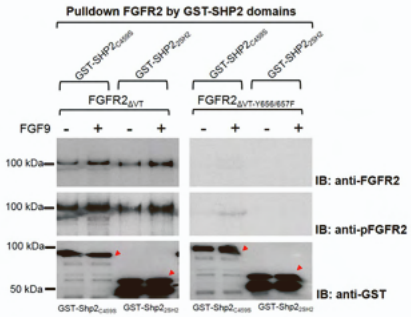

B

Figure 4B replicate 2

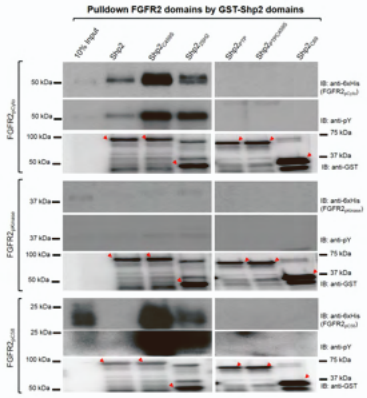

C

Figure 4C replicate 2

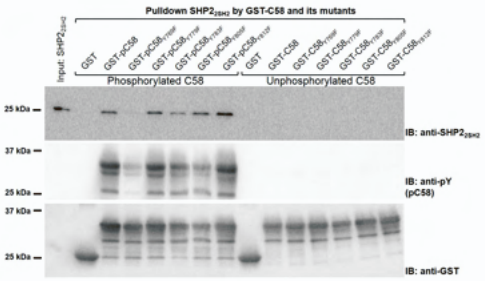

Figure 4C replicate 3

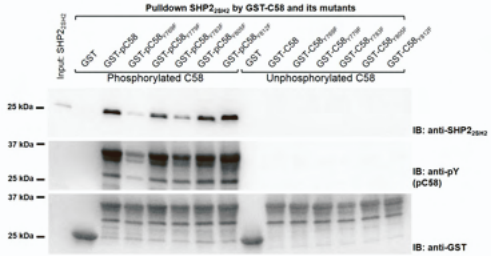

Figure 4C replicate 4

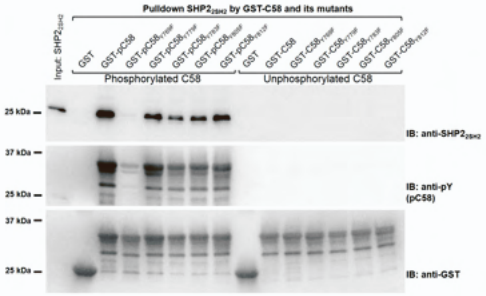

D

Figure 4D replicate 2

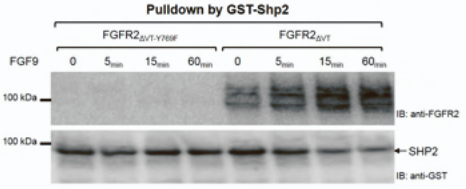

Figure 4D replicate 3

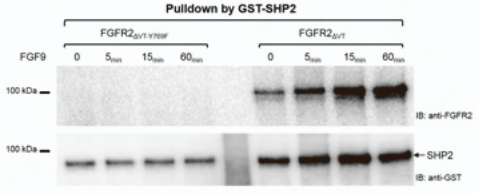

E

Figure S4E replicate 2

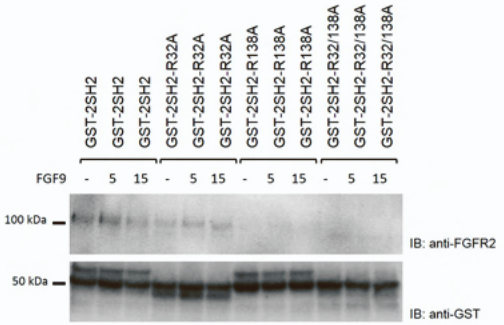

Data S2. Replicated western blots, Related to Figure 5 and Figure 6.

A

Figure 5E replicate 2

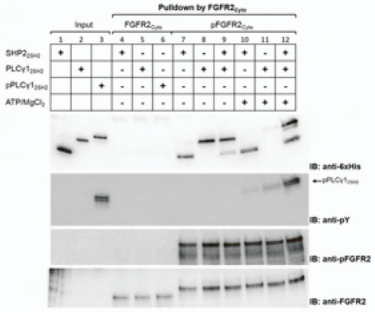

Figure 5E replicate 3

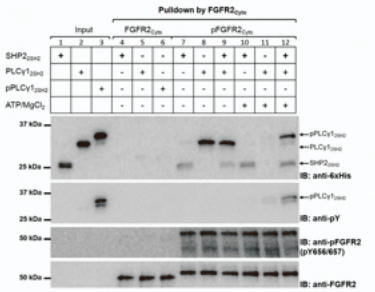

B

Figure 6D replicate 2

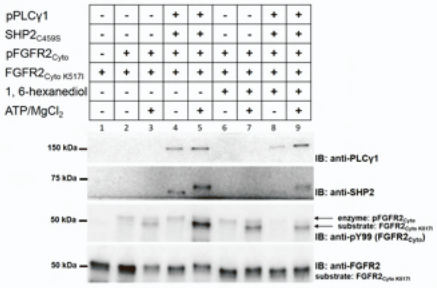

Figure 6D replicate 3

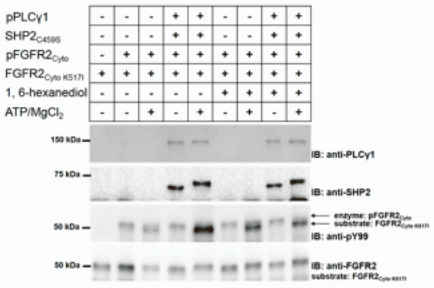

Figure 6D replicate 4

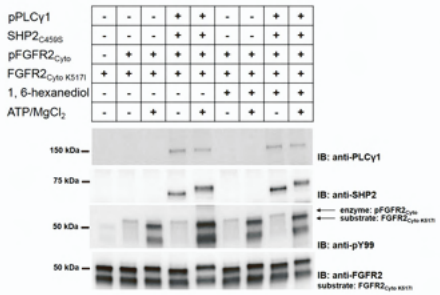

Figure 6D replicate 5

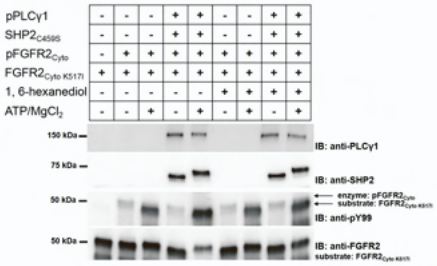

C

Figure 6E replicate 2

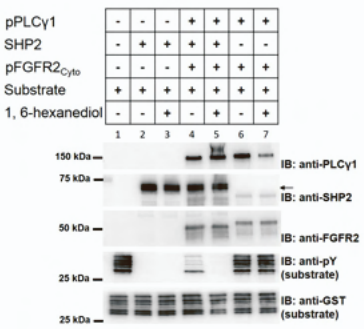

D

Figure 6F replicate 2

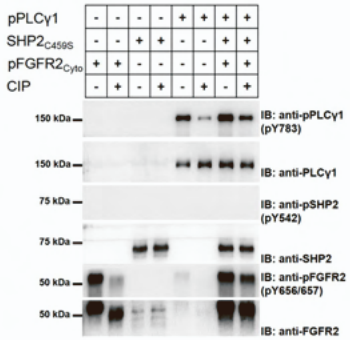

Data S3. Replicated western blots, Related to Figure 7 and Figure S7.

A

Figure 7A (MCF7) replicate 2

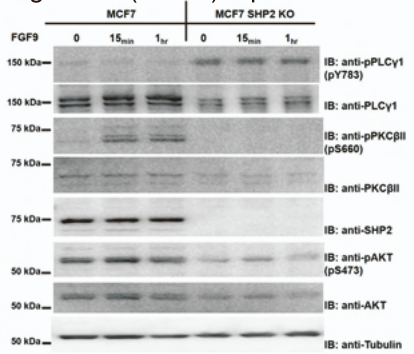

Figure 7A (MCF7) replicate 3

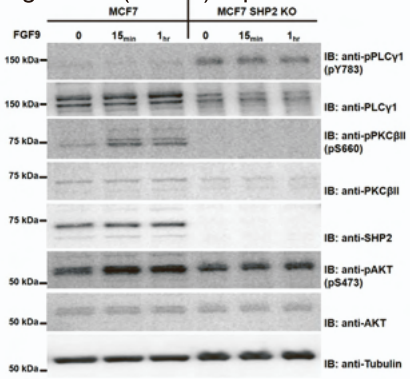

Figure 7A (A431) replicate 2

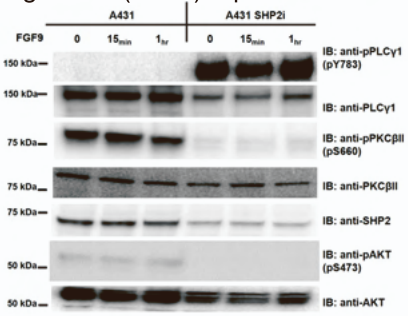

B

Figure 7D replicate 2

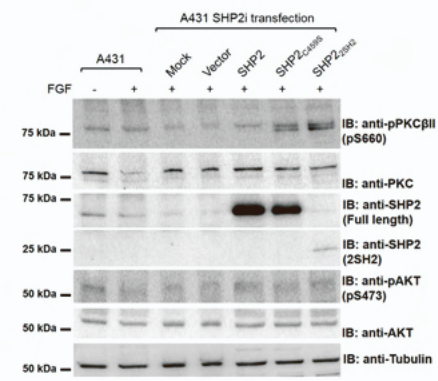

Figure 7D replicate 3

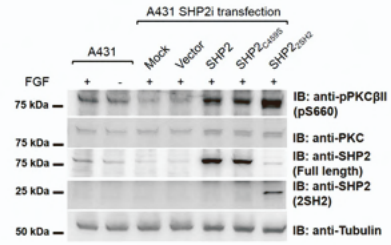

C

Figure 7E replicate 2

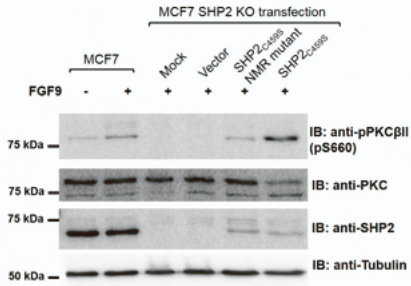

Figure 7E replicate 3

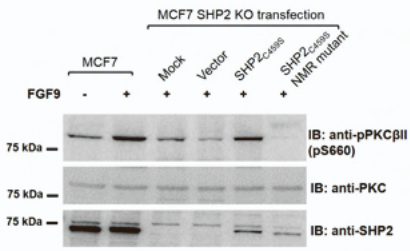

D

Figure S7A replicate 2

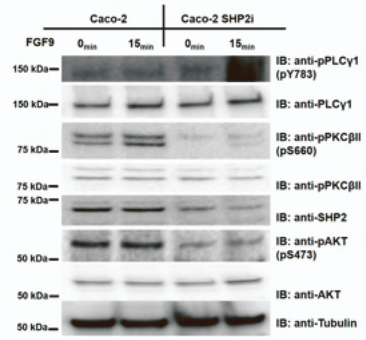

E

Figure S7B replicate 2

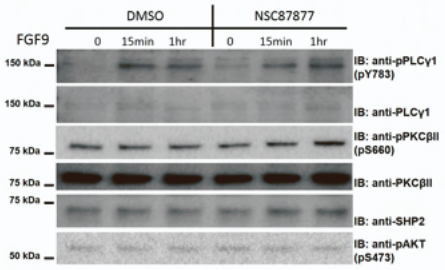

Figure S7B replicate 3

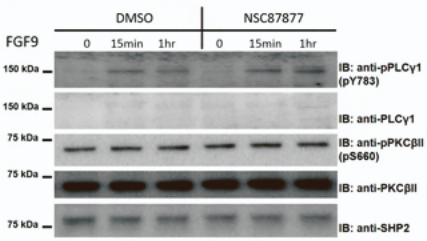

F

Figure S7C replicate 2 and 3